Appl. Phys. B
DOI 10.1007/s00340-015-6051-y

Applied Physics B
Lasers and Optics

Performance tolerance analysis of birefringent fiber loop for semiconductor optical amplifier pattern effect suppression

Zoe V. Rizou · Kyriakos E. Zoiros · Antonios Hatziefremidis · Michael J. Connelly

Received: 18 December 2014 / Accepted: 13 February 2015

Abstract In this paper, we analyze the performance of the birefringent fiber loop (BFL) when the settings of the components that construct this module are not perfect. The BFL is employed for suppressing the pattern effect on directly amplified data in a semiconductor optical amplifier (SOA). The analysis is conducted by describing the non-optimum BFL transmission response using Jones matrix method. This allows to formulate a comprehensive model, which is validated by comparing it to the experiment. Then we investigate and specify how sensitive the BFL is to imperfections of its building components by assessing its performance against the output amplitude modulation, power penalty, and crosstalk. For each critical operating parameter, we derive the tolerance range within which these performance metrics are acceptable. The obtained results suggest that the BFL can efficiently mitigate the SOA pattern effect even if it is built from non-ideal components. This can be achieved provided that these components are designed according to their extracted operating conditions, which are practically satisfiable.

Keywords Birefringent fiber loop · Modeling · Pattern effect · Semiconductor optical amplifier

Z. V. Rizou · K. E. Zoiros (✉)
Department of Electrical and Computer Engineering, Democritus University of Thrace, 67 100 Xanthi, Greece
e-mail: kzoiros@ee.duth.gr

Z. V. Rizou
e-mail: zrizou@ee.duth.gr

A. Hatziefremidis
Department of Aircraft Technology, Technological Educational Institute of Chalkis, Chalkis, Greece
e-mail: ahatzi@teihal.gr

M. J. Connelly
Optical Communications Research Group, Department of Electronic and Computer Engineering, University of Limerick, Limerick, Ireland
e-mail: michael.connelly@ul.ie

1 Introduction

Owing to its passive nature, simple structure, low cost, compatibility with fiber medium, robustness to environmental perturbations, polarization independence, notable peak-to-notch contrast ratio, periodic transfer function, and flexibly tunable transmission characteristics, the birefringent fiber loop (BFL) has been widely employed as frequency discriminator in a wide range of applications in the optical domain [1]. These include optical pulse generation [2], repetition rate multiplication [3], development of multi-wavelength laser sources [4, 5], reduction of amplitude transients [6], all-optical clock recovery [7], wavelength conversion [8], differential phase shift keying (DPSK) demodulation [9], demultiplexing [10], Boolean logic [11], and sensors [12]. In this context, we have recently shown that a BFL can also be exploited to suppress the pattern effect induced on 10 Gb/s return-to-zero (RZ) data pulses that are directly amplified by a semiconductor optical amplifier (SOA) [13, 14]. The main goal of this work has been to demonstrate the feasibility and proof of principle using the BFL for the specific purpose. However, the operation of the BFL, which in this case was configured as notch filter, critically depends on the deviation of its building components from their ideal settings [1]. Thus, it would be practically interesting to investigate and assess how sensitive and tolerant is the performance of the BFL-based scheme to these imperfections. Furthermore,

Published online: 05 March 2015

it would be useful to quantitatively know what degree of freedom is allowed when designing and constructing the BFL for the intended target. In the present paper, this goal is achieved by means of numerical simulation and analysis, which takes into account the finite resolution of the relative delay between the axes of the polarization maintaining fiber (PMF), the non-optimum adjustment of the intraloop polarization controller (PC), and the asymmetric power splitting ratio of the optical coupler (OC) that forms the BFL. By conducting this study, we manage to specify the permissible range of values for the key BFL components parameters. To this end, our findings suggest that the BFL can efficiently mitigate the SOA pattern effect even if it is built from non-ideal components. For this purpose, these components must be designed to comply with their extracted operating conditions, which are practically feasible.

2 Background

Figure 1 shows schematically the configuration in which a BFL is connected to the output of a SOA. A random data stream is inserted into the SOA to undergo amplification. In this case, the profile of the output signal should ideally be an amplified replica of the input one. However, the SOA has a finite gain recovery time, and so its response to this excitation is not instantaneous. Moreover, when the input data have high peak power and large duty cycle, the SOA gain drops well below the unsaturated gain [15] and the amplification experienced by a given bit depends on the previous bits. As a result, pulses that occupy a fraction of the repetition interval are not uniform at the SOA exit but suffer from peak amplitude fluctuations [15].

The pattern-dependent pulse wandering affects negatively the performance characteristics of SOAs employed for pure amplification purposes. These characteristics include amplitude modulation, Q-factor, optical signal-to-noise ratio, output power, in-line spacing, and input power dynamic range [15, 16]. Therefore, compensating for this problem is imperative in order to enable the unobstructed use of SOAs for direct amplification applications. One

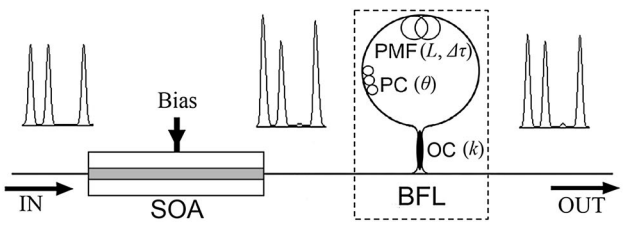

Fig. 1 SOA and BFL configuration. OC: optical coupler of splitting ratio k, PC: polarization controller of rotation angle θ, PMF: polarization maintaining fiber of length L and delay $\Delta\tau$

method that can be adopted for this purpose exploits the spectral broadening of the amplified pulses to longer wavelengths (red shift) due to self-phase modulation (SPM) [17]. More specifically, the amount of the SPM-induced spectral shift to longer wavelengths is larger for the higher than for the lower-amplitude marks. This suggests that if a large part of the broadened spectrum after the SOA is selected for the less intense marks, while it is rejected for the more intense marks, then the uneven red shift can be compensated and converted into more equalized pulse peak amplitudes. The achievement of this goal requires resorting to some type of optical filtering [15, 18–24]. In this context, we have shown how the BFL can successfully act as notch filter to mitigate the SOA pattern effect [13, 14].

In its standard structure, the BFL consists of an OC, a PC, and a PMF [1]. Each one of these building components plays a distinctive role in the operation of the BFL. First, the coupler of cross-coupling power ratio k splits the incoming data modulated light wave into two counter-propagating beams, which reenter it after travelling along identical optical paths inside the loop. Secondly, the PC changes the orientation of the linearly orthogonal polarization states, into which each beam is decomposed, by some angle θ between 0 and $\pi/2$ with respect to one of the principal axes of the PMF. Thirdly, the PMF of length L introduces via its birefringence B a relative delay, $\Delta\tau = (BL)/c$, where c is the speed of light in vacuum, and accordingly a wavelength-dependent phase difference between these polarization components, $\Gamma(\lambda) = (2\pi c\Delta\tau)/\lambda = (2\pi BL)/\lambda$, where λ is the reference wavelength [1].

The OC should equally divide the signal received by the BFL, while the PC should produce a rotation of $\pi/2$ to the polarization of light coming from both directions. This implies that k and θ should obey $k = 0.5$ and $\theta = 90°$. In this case, the intensity transmission function at BFL output port 2 is given in the spectral domain by [1]

$$T_{\mathrm{BFL}}(\lambda) = \cos^2[\Gamma(\lambda)/2] = \cos^2[\pi \mathrm{BL}/\lambda] \tag{1}$$

This function exhibits repetitive lobes, which alternate between maxima (peaks) and minima (notches) in a comb-like manner [1]. The wavelength separation between consecutive maxima is determined by the free spectral range (FSR), $\mathrm{FSR} = \lambda^2/(c\Delta\tau) = \lambda^2/(\mathrm{BL})$ [1], while the minima are located halfway between them. The cosine-squared form of the spectral response enables the BFL to be employed as notch filter for suppressing the SOA pattern effect [13, 14]. However, if the OC and PC deviate from their optimum settings, the potential of the BFL to improve the pattern-dependent SOA performance can be seriously compromised. In practice, this can happen when the coupler does not have a perfect 3 dB power-coupling coefficient due either to uncertainties in the manufacturing process or to its wavelength dependence [25], and also because

the PC has limited precision when it is manually controlled [9]. The consequences of these imperfections are twofold. First, the relative contrast between the BFL transmission maximum and the adjacent minimum is reduced [1]. In section 3, we show through Jones matrix description the exact magnitude of this reduction as function of k and θ. Then, the asymmetrically broadened spectral components after the SOA will not be properly aligned around the notches but lie closer to the BFL transmission peak. Thus, they will suffer only a partial and identical attenuation, when the latter should scale with the degree of their red shift [15]. Second, the power of the polarization mode to which the incident amplified light is transferred at the BFL output [6–8] is decreased. This manifests as unwanted crosstalk between the orthogonal states of polarization. The amplified signal will then suffer a stronger elimination due to the filtering action of the BFL [23]. This leads to reduction in the net gain of the SOA-BFL combination, which will not be sufficient for supporting ultrafast direct signal amplification with network loss compensation included [15]. On the other hand, the PMF differential time delay, $\Delta\tau$, may fluctuate if the PMF is subject to environmental changes, especially of the ambient temperature [26], or if the PMF suffers various mechanical strains, such as bending, tension, or twist [27] during manufacturing or handling. The finite accuracy of providing this temporal offset may also be affected if the PMF is connected to the two branches of the polarization-preserving coupler by splicing or is formed by concatenating different PMF segments [27]. This may disturb the condition of interference of the recombined counter-propagating amplified signal constituents [28]. Consequently, it may not be possible for the higher amplified marks to be clamped and the lower ones to be comparatively enhanced, as required in order to suppress the SOA pattern effect [22]. This fact will result in a high-amplitude modulation and hence in an unacceptable degree of pattern effect at the cost of increased power penalty [20]. Therefore, if any of the above practical reasons holds, either individually or in combination, then the efficiency of the BLF scheme to suppress the SOA pattern effect will be reduced. Therefore, the impact of the non-ideal PMF, PC, and OC must be considered, investigated, and assessed. This task is addressed in the following by conducting numerical modeling and deriving simulation results.

3 Modeling

In order to model the setup in Fig. 1, we describe first the BFL operation and then link it to the SOA operation. For this purpose, we follow a fundamental theoretical approach, which relies on working with electric fields so as to be able to pass from the time to the spectral domain, and vice versa, and acquire information in both domains. The objective is to obtain expressions for the electric field of the signal after the SOA and after the BFL.

The transmission of a comb filter, like the BFL, can be conveniently modeled by means of Jones matrix formalism [28–34]. For this purpose, we must identify the Jones matrix of each element involved in the construction of the BFL. Thus, starting with the 2×2 OC, and assuming that it is a polarization-independent reciprocal element, its Jones matrix is [31]

$$[K_I] = \begin{bmatrix} \sqrt{1-k}[I] & j\sqrt{k}[I] \\ j\sqrt{k}[I] & \sqrt{1-k}[I] \end{bmatrix} \tag{2}$$

in the direction of splitting light and

$$[K_C] = \begin{bmatrix} j\sqrt{k}[I] & \sqrt{1-k}[I] \\ \sqrt{1-k}[I] & j\sqrt{k}[I] \end{bmatrix} \tag{3}$$

in the direction of combining light. In these relationships, $[I]$ is the identity matrix while the imaginary number unit j stands for the cross-coupling pass of light in both directions and the induced phase shift of $\pi/2$ relative to in-coupling. Proceeding with the PC, its Jones matrix is [28]

$$[J_{\mathrm{PC}}] = \begin{bmatrix} \cos\theta & -\sin\theta \\ \sin\theta & \cos\theta \end{bmatrix} \tag{4}$$

Finally, the Jones matrix of the PMF is [28, 30–32]

$$[J_{\mathrm{PMF}}] = \begin{bmatrix} e^{j\Gamma(\lambda)/2} & 0 \\ 0 & e^{-j\Gamma(\lambda)/2} \end{bmatrix} \tag{5}$$

The BFL can be described by taking the product of these matrices according to the rules of Jones calculus [35]. This is separately done for the clockwise and counterclockwise directions [32, 33] according to the equivalent optical circuit of the employed BFL configuration [30]. By combining the resultant Jones matrices and using the same nomenclature as in [34] for light propagation through the BFL, we obtain the relationship between the output and input electric fields

$$\begin{bmatrix} [E1_{\mathrm{OUT}}] \\ [E2_{\mathrm{OUT}}] \end{bmatrix} = [K_C] \times \begin{bmatrix} [J_{\mathrm{PMF}}][J_{\mathrm{PC}}] & [0] \\ [0] & [J_{\mathrm{PC}}]^T[J_{\mathrm{PMF}}]^T \end{bmatrix} \times [K_I] \times \begin{bmatrix} [E1_{\mathrm{IN}}] \\ [E2_{\mathrm{IN}}] \end{bmatrix} \tag{6}$$

In the general case, $[E1_{\mathrm{IN}}], [E2_{\mathrm{IN}}], [E1_{\mathrm{OUT}}]$ and $[E2_{\mathrm{OUT}}]$ are two-dimensional column vectors, which describe the input and output electric fields at BFL input port 1 and output port 2, respectively. However, with regard to the experiment [13, 14], only port 1 receives light. In practice, this condition is satisfied owing to the small polarization sensitivity of commercial SOA devices [36], and the fact that the transmission of the BFL is independent of the input polarization [6]. Thus, without loss of generality, we can

assume that the data modulated light which exits the SOA and enters the BFL is linearly polarized along the horizontal PMF axis, x. This means that $[E1_{\mathrm{IN}}] = \begin{bmatrix} E1_{\mathrm{IN},x} & 0 \end{bmatrix}^T$ and $[E2_{\mathrm{IN}}] = [0]$, where the superscript 'T' denotes the transpose matrix operator, which is applied to account for beam counter-propagation [32, 33], and [0] is the null matrix. After algebraic manipulation of (6), we can derive the expression at BFL output port 2 for the electric field component whose polarization should be swapped, according to the BFL principle of operation [6, 7], to the vertical PMF axis, y

$$E2_{\mathrm{OUT},y}(\lambda) = [e^{-j\Gamma(\lambda)/2}\sin\theta + 2jk\sin(\Gamma(\lambda)/2)\sin\theta]E1_{\mathrm{IN},x}(\lambda) \tag{7}$$

However, in case that $k \neq 0.5$ and $\theta \neq 90°$, part of the input electric field at the original polarization, x, is also transmitted to the target BLF output port 2, as indicated by

$$E2_{\mathrm{OUT},x}(\lambda) = (1-2k)\cos\theta e^{j\Gamma(\lambda)/2}E1_{\mathrm{IN},x}(\lambda) \tag{8}$$

Since this term can be completely extinguished only when $k \neq 0.5$ and $\theta \neq 90°$, this means that it reduces the total intensity at the output. This negative effect is taken into account in the BFL performance tolerance analysis through the quantity of crosstalk, as highlighted in Sect. 5. Thus, by adding the squared modulus of (7) and (8) and normalizing the sum to the input, the intensity transmission at BFL output port 2 is

$$\begin{aligned} T'_{\mathrm{BFL}}(\lambda) &= \left[\left|E2_{OUT,y}(\lambda)\right|^2 + \left|E2_{\mathrm{OUT},x}(\lambda)\right|^2\right] / \left|E1_{\mathrm{IN},x}(\lambda)\right|^2 \\ &= 1 + 4k(k-1)[1 - \sin^2\theta\cos^2(\Gamma(\lambda)/2)] \end{aligned} \tag{9}$$

This is the general form of the BFL transfer function which includes the contributions of all BFL building components when these are non-ideal.

From (7) and (8), the electric fields at BFL output port 2 can be converted back into the time domain through

$$E2_{\mathrm{OUT},y}(t) = F^{-1}\left\{F[E_{\mathrm{SOA}}(t)]\left[E2_{\mathrm{OUT},y}(\lambda)/E1_{\mathrm{IN},x})(\lambda)\right]\right\} \tag{10}$$

$$E2_{\mathrm{OUT},x}(t) = F^{-1}\left\{F[E_{\mathrm{SOA}}(t)]\left[E2_{\mathrm{OUT},x}(\lambda)/E1_{\mathrm{IN},x})(\lambda)\right]\right\} \tag{11}$$

where the operators F and F^{-1} stand for Fast Fourier Transform (FFT) and the inverse operation (IFFT), respectively, and $E_{\mathrm{SOA}}(t)$ is the electric field of the amplified data, which is normalized so that its squared modulus represents power [17]. This is given by $E_{\mathrm{SOA}}(t) = E_{data}(t)\exp\left[{}^1/_2(1-j\alpha)h(t)\right]$, where $\alpha = 8$ is the SOA linewidth enhancement factor [15] and $h(t)$ is the integrated SOA power gain in response to data of amplitude $E_{\mathrm{data}}(t)$ [17]. This function satisfies the following differential equation

$$\frac{\mathrm{d}h(t)}{\mathrm{d}t} = \frac{\ln(G_{\mathrm{ss}}) - h(t)}{T_{\mathrm{carrier}}} - \frac{|E_{\mathrm{data}}(t)|^2}{E_{\mathrm{sat}}}\{\exp[h(t)] - 1\} \tag{12}$$

where $G_{\mathrm{ss}} = 23\,\mathrm{dB}, T_{\mathrm{carrier}} = 75\,\mathrm{ps}, E_{\mathrm{sat}} = 1.5\,\mathrm{pJ}$ are the SOA small signal gain, carrier lifetime, and saturation energy, respectively. The solution of (12) according to the numerical approach described in [37] and for the same input data signal characteristics as in [15] allows to calculate $h(t)$. By knowing $h(t)$, we can then find the signal power, $P_{\mathrm{SOA,BFL}}(t) = \left|E_{\mathrm{SOA,BFL}}(t)\right|^2$, and spectrum, $S_{\mathrm{SOA,BFL}}(\lambda) = \left|F\left[E_{\mathrm{SOA,BFL}}(t)\right]\right|^2$, after the SOA and BFL, respectively, where $|E_{\mathrm{BFL}}(t)|^2 = \left|E2_{\mathrm{OUT},y}(t)\right|^2 + \left|E2_{\mathrm{OUT},x}(t)\right|^2$ using (10) and (11). The modeling is executed in MATLAB.

4 Model validation

We first demonstrate the suitability of the model to produce realistic and accurate results. Since for the SOA this task has been successfully addressed in [15, 37], in the following, we focus on whether this validity also holds for the theoretical description of the BFL. For this purpose, we compare theoretical against experimental data [13, 14] so to check whether there is a good agreement between them.

Starting with the BFL spectral response, we show in Fig. 2 the measured (solid line) and the calculated (dashed line) intensity transmission spectra. Both results are obtained for $\Delta\tau = 8.8$ ps used in the experiment [13, 14]. Since during the experiment the PC inside the BFL was manually controlled, it was not possible to know precisely

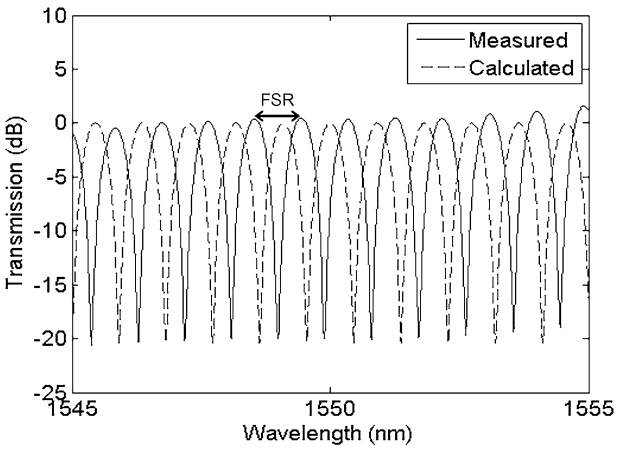

Fig. 2 Measured (*solid line*) and calculated (*dashed line*) BFL intensity transmission spectra. FSR: free spectral range

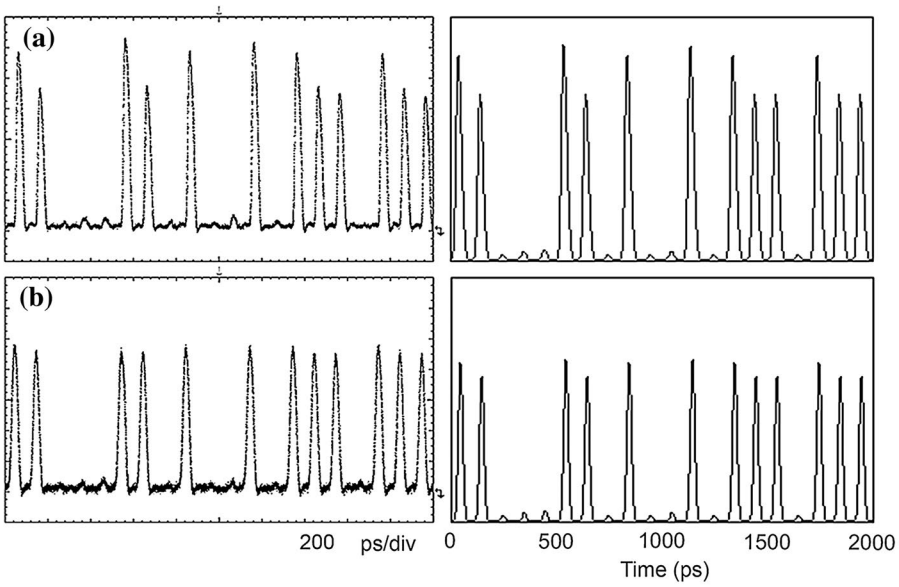

Fig. 3 Temporal waveforms for data with initial pattern effect at **a** SOA output and **b** BFL output. *Left column*: experimental results [13]. *Right column:* simulation results

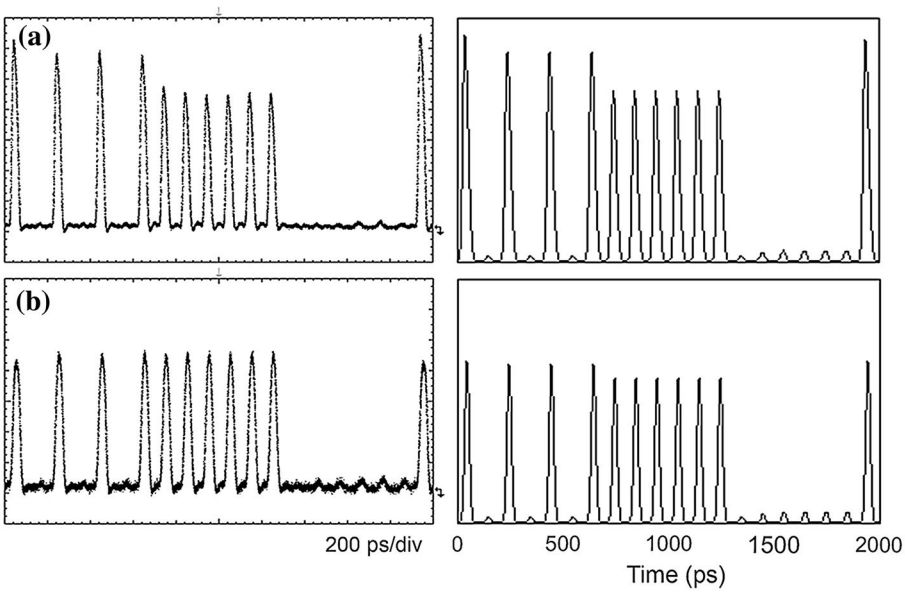

Fig. 4 Temporal waveforms for data with an interval of six consecutive spaces in between marks at **a** SOA output and **b** BFL output. *Left column:* experimental results [14]. *Right column*: simulation results

the rotation angle θ. The BFL OC had a power-coupling tolerance whose exact percentage was not known either, and so k could deviate from being purely symmetric. For these reasons, the BFL transmission could not be optimized according to (1). Instead, the best interference fringe achieved had a finite peak-to-notch contrast ratio (PNCR) of ≈ 20.5 dB around 1550 nm [13, 14]. According to (9),

$$\mathrm{PNCR} = \frac{T'_{\mathrm{BFL,max}}}{T'_{\mathrm{BFL,min}}} = \frac{1 + 4k(k-1)\cos^2\theta}{1 + 4k(k-1)}, \quad k \neq 1/2 \tag{13}$$

where $T'_{\mathrm{BFL,max}}$ and $T'_{\mathrm{BFL,min}}$ denotes the maximum (peak) and minimum (notch), respectively, of the BFL transfer function. Thus, by setting this ratio equal to 20.5 dB, we find $\theta \approx 89.8°$ and $k \approx 0.452$, which are used as fixed values for these parameters throughout the simulation. Next, we replace these values in (9) and plot the simulated transfer function, $T'_{\mathrm{BFL}}(\lambda)$, together with its experimental counterpart. In this procedure, the analytical result has been derived by assuming that the losses of the components that construct the BFL are compensated for. In practice, this condition is satisfied with the assistance of external amplification [13–15]. Then, we can see that, except for slight discrepancies in the characteristics of the peaks and notches, which occur for similar reasons to those justified in [15], the forms of the two curves are identical, which confirms the correctness of (9).

We continue by addressing the correctness of (10) and (11). Since the sum of their squared moduli results in $|E_{\mathrm{BFL}}(t)|^2$, this is done with the help of the experimental evidence available for the BFL outcome in the time domain [13, 14]. More specifically, Figs. 3 and 4 depict temporal waveforms at the SOA (a) and BFL (b) output for a representative 20-bit-long data stream inside a pseudorandom binary sequence (PRBS) of word length 2^7-1. This data stream contains pulses that either have an initial amplitude modulation of 0.35 dB [13, 14] prior to entering the SOA (Fig. 3), or are separated by an interval of six consecutive spaces [14] (Fig. 4). Then, we can verify that in both cases, there is a good agreement between experimental (left column) and theoretical results (right column). In fact, the numerically calculated amplitude modulation values after the BFL, namely 0.28 dB (Fig. 3b) and 0.23 dB (Fig. 4b), are comparable to those reported in [13, 14]. Furthermore, the profile of the simulated pulses and of their amplitude fluctuation is similar to experiment.

5 Results and discussion

The sensitivity and tolerance of the BFL-based SOA pattern effect suppression scheme to the deviation of the BFL components from their optimum settings is investigated and assessed against the following performance criteria. First, the amplitude modulation (AM) of the output signal, which quantifies the pattern-dependent pulse wandering. It is defined as AM (dB) $= 10\log(P^1_{\max}/P^1_{\min})$, where $P^1_{\max}$ and $P^1_{\min}$ is the maximum and minimum peak power of the marks in the amplified data stream, respectively [22]. The AM should be as low as possible but it is considered acceptable for lightwave telecommunication systems if it is lower than 1 dB [22]. Second, the crosstalk (CT) at the BFL output, which is defined as CT (dB) $= 10\log\left(|E2_{\mathrm{OUT},x}|^2/|E2_{\mathrm{OUT},y}|^2\right)$, and is a measure of the degree of signal isolation between the desirable, y, and undesirable, x, polarization modes [38]. Third, the power penalty (PP), which characterizes how efficiently the BFL can achieve error-free operation. It is defined as the difference in the average optical power at the receiver end between the back-to-back (b-b) and BFL connection, in order for the Q-factor to equal six, i.e., $Q = 6$, or equivalently for a bit-error rate BER $= 1\times10^{-9}$ [39]. By neglecting the contribution of the spaces to the receiver performance for reasons explained in [15], this metric is calculated in the thermal noise limit from [39] $Q = 2R\overline{P}_{\mathrm{rec,BFL}}/\sigma_{1,\mathrm{tot}}$, where $\overline{P}_{\mathrm{rec,BFL}}$ is the average received power after the BFL, $R = 1$ A/W is the receiver responsivity at 1550 nm and $\sigma_{1,\mathrm{tot}}$ is the root-mean-square value of the total noise current fluctuation induced due to the pattern effect and the receiver thermal noise. Thus, the variance of this quantity is given from $\sigma^2_{1,\mathrm{tot}} = \sigma^2_{1,\mathrm{pe}} + \sigma^2_T$, where $\sigma^2_{1,\mathrm{pe}}$ is the variance of the peak powers of the marks caused due to the pattern effect, and [39] $\sigma^2_T = (4k_BT/R_L)F_n\Delta f$ is the thermal noise variance, where k_B is Boltzmann's constant, T is the absolute temperature, and $R_L = 50\,\Omega, F_n = 2$ (3 dB) and $\Delta f = 5$ GHz are the receiver's load resistor, noise figure and bandwidth, respectively. Then $\overline{P}_{\mathrm{rec}}$ is calculated for the target Q-factor for different BFL critical parameters settings and is compared to the back-to-back receiver sensitivity, $\overline{P}_{\mathrm{rec},b-b} = Q\sigma_T/R$ [39]. The PP is found after accounting for the contribution to the power budget from components such as booster amplifiers, attenuators, filters, and couplers, which intervene in the fiber path that leads to the receiver for the BER measurements [15]. Ideally, the PP must be as low as possible, still if it does not exceed 1 dB, then it lies well within the typical range of values allocated for lightwave system performance degradation impairments [40]. In the following, we present simulation results against $\Delta\tau, \theta$ and k so as to specify if, and under which conditions, all defined performance criteria can be simultaneously met. Note that the impact of the non-ideal OC is also quantified through the percentage deviation from the perfect 3 dB splitting ratio, Δ. This percentage is related to the cross-coupling power coefficient, $k \le 0.5$, by $k = 0.5(1-\Delta)$ [41], so that $\Delta = 0$ corresponds to a perfectly symmetric coupler, $k = 0.5$.

Figure 5 shows the variation of the AM against $\Delta\tau$. This curve was obtained for an initial pulse AM, so that the AM after the SOA is equal to the experimental one [13, 14]. This was done because during the experiment, the AM was measured on pulses that belonged to the 20-bit-long data stream of Fig. 3a, while in the simulation the AM was

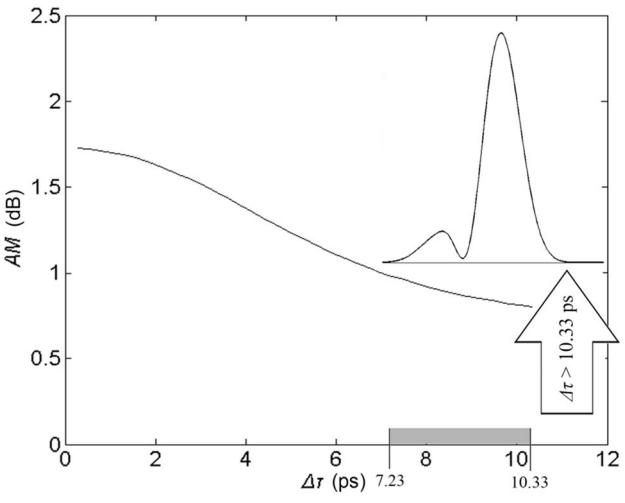

Fig. 5 Variation of amplitude modulation, AM, versus PMF relative delay, $\Delta\tau$. The *gray zone* indicates the permissible range of values for this parameter. The *vertical arrow* indicates the limit above which pulse distortion occurs due to BFL filtering

calculated across the whole PRBS. From this figure, we observe that the AM is gradually reduced with the increase of $\Delta\tau$. This occurs because the FSR and the falling slope of the BFL transfer function become more narrow and steep, respectively. These changes enable the BFL to compensate more efficiently for the pattern effect. This behavior was explained for polarization discrimination-based filtering schemes having similar operation principle and intended to serve the same purpose as the BFL [15]. However, as $\Delta\tau$ continues to increase and the equivalent PMF length exceeds 10 m, a satellite pulse appears inside the bit interval of the amplified pulses. This impairs their profile, as shown in Fig. 5, and imposes a bound on the maximum possible AM reduction.

The dependence of the PP on $\Delta\tau$ is shown in Fig. 6. This curve was obtained by running the SOA model after adding 31 repetitive marks before applying the standard 2^7-1 PRBS. This bit padding was necessary because the BER and subsequently the PP measurements were taken by using a PRBS of length $2^{31}-1$ [13, 14]. However, employing such a long PRBS would be prohibitive for the simulation in terms of computational efficiency [42]. To overcome this difficulty but still ensure that the SOA is driven by data under a similarly demanding condition, we exploited the PRBS balance property. According to this property, the longest run of marks in a PRBS of length 2^n-1 is n [43]. In this manner, we managed to simulate the perturbation of the SOA gain dynamics by the same number of consecutive marks as in the laboratory and hence evaluate the PP when the SOA pattern-dependent operation is stressed on the edge. Since in this case the SOA is heavily saturated, its recovered gain at the end of the applied string of marks,

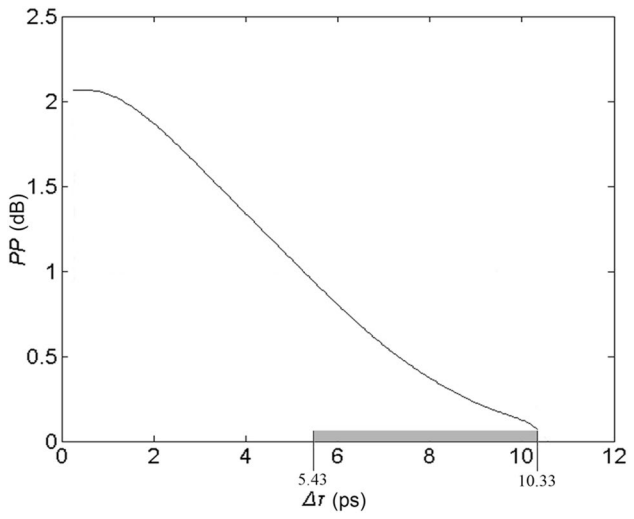

Fig. 6 Variation of power penalty, PP, versus PMF relative delay, $\Delta\tau$. The *gray zone* indicates the permissible range of values for this parameter

G_0, is well below the unsaturated level, G_{ss}. This reduced gain defines the initial gain encountered by the first sample of the first pulse in the 2^7-1 long PRBS. For this reason, (12) was solved to find the SOA response, $h(t)$, by replacing G_{ss} with G_0. By following this approach, the amount of simulated PP right after the SOA, i.e., for $\Delta\tau = 0$ ps, was fitted to the experimental one [13, 14]. However, the predicted PP reduction owing to the BFL is somewhat higher than the experimental one [13]. This designates that there is margin for further improvement of the PP. In fact, the form of the curve shows that as $\Delta\tau$ is increased, the PP follows the AM drop in Fig. 5 but more sharply. Moreover, the PP becomes acceptable when $\Delta\tau$ is 1.8 ps smaller than for the AM. These observations indicate that the PP is actually more sensitive to the variations of the specific parameter. The power penalty reaches its minimum, PP = 0.07 dB, at the rightmost side of the horizontal axis, i.e., for $\Delta\tau = 10.33$ ps, where the amplitude modulation exhibits its lowest level, AM = 0.8 dB. Thus, both metrics become minimum, but the magnitude of the AM is comparatively larger. Nevertheless, even when the amplified data pulses must drive another SOA, as it happens in cascaded SOA architectures [44], another BFL can compensate for the AM imposed on these data pulses so that it is well below 1 dB before entering the next SOA.

According to Figs. 5 and 6, the upper edge of $\Delta\tau$ values is common for PP and AM, while the lower edge is determined by the AM. Thus, the values of $\Delta\tau$ which are permissible for both PP and AM span from 7.23 to 10.33 ps, which means that $7.23 \leq \Delta\tau \leq 10.33$ ps. Interestingly, the value of $\Delta\tau$ that we used in the experimental demonstration in [13, 14] falls inside this range, which supports the validity of the above extracted condition. Now, we must check whether this range is sufficient from a practical perspective and also suitably select a $\Delta\tau$ within it. $\Delta\tau$ may fluctuate due to reasons associated with the loop length or birefringence. In the BFL conventional implementation, the length of the PMF may not be accurately known due to uncertainties, either when this length is experimentally measured, or when the PMF is manufactured. In the former case, the maximum deviation from the correct $\Delta\tau$ value is of the order of 0.125 ps. This value is estimated for a commercially available PMF patchcord as short as 0.25 m, assuming that the committed measurement error is as high as half the nominal value. In the latter case, the maximum deviation of $\Delta\tau$ is of the order of 0.1 ps as a result of a typical PMF length tolerance ± 10 cm specified in data sheets. Moreover, the PMF length and birefringence may undergo perturbations due to changes in ambient temperature [26]. However, the respective thermal expansion and thermo-optic coefficients in response to these changes are of the order of 10^{-7} per degree celsius [26, 45]. This means that the temporal displacement of $\Delta\tau$ is negligible, much more

if a PM photonic crystal fiber (PCF), which is extremely insensitive to temperature variations [26], is used instead of the standard PMF. $\Delta\tau$ also drifts due to strain-induced birefringence changes, which are applied via the intraloop PC in order to properly detune the BFL transmission peak and efficiently suppress the SOA pattern effect [13, 14]. Again, a very small alteration of the loop birefringence, i.e., $\approx 10^{-7}$, is adequate for shifting the comb spectrum by FSR/2 [46]. On the other hand, a more convenient and compact way to emulate the function of the PMF is to replace it by a differential polarization delay line (DPDL) [15]. The resolution of such an off-the-shelf module can be as high as 1.36 ps when the delay is varied as fast as a quarter of a millisecond [47]. Therefore, among all the aforementioned factors that incur a change on $\Delta\tau$, the contribution of the finite DPDL resolution is the highest and accordingly determines the maximum tolerance of the central $\Delta\tau$ value, i.e., ± 1.36 ps. Then we choose the upper bound of $\Delta\tau$ as the reference point. The reason for doing this is because this bound is the more restrictive for the performance of the BFL scheme due to the serious pulse deformation that occurs if it is surpassed. In this manner, we take $\Delta\tau = 8.97$ ps. This value is only ≈ 2 % higher than that in [13, 14] and ensures that the various fluctuations of $\Delta\tau$ are confined within the derived allowable range of this critical parameter.

The effect of the PC orientation angle on the BFL performance metrics is investigated by altering θ up to 10° away from its optimum value of 90°. Initially, we verify that the variation of the specific parameter within this range does not cause any distortion of the amplified pulses nor has a significant impact on the AM, which remains almost constant to the acceptable value of 0.87 dB. However, this does not happen for the CT, as shown in Fig. 7, since as θ is reduced from $\pi/2$, the *CT* is progressively increased. When θ drops below 86.85°, the CT becomes higher than 40 dB. If the latter value is taken as the reference limit, then the maximum deviation of the rotation angle, $\Delta\theta_{\max}$, from its ideal setting that can be tolerated with respect to the CT is 3.15°. This is an important difference against $\Delta\tau$, despite the variations of which CT is kept well below 40 dB. Furthermore, we note that the specified permissible margin can be even narrower if the criterion for the CT becomes more tight, i.e., $\approx 0.32°$ at 60 dB. Nevertheless, $\Delta\theta_{\max}$ is still practically achievable with electrically, instead of manually, actuated PCs, which can have a rotational accuracy as fine as 0.225° at the price of a more complicated and less cost-effective construction [48]. Concurrently, the incurred PP does not exceed 0.3 dB, and hence, it is more than acceptable.

The sensitivity of the BFL performance to the variation of the coupling coefficient is checked with the help of Figs. 8 and 9. It can be seen that the asymmetric splitting ratio can be reduced until $k < 0.23$, where the PP is intolerably degraded. However, the allowable variation is much smaller with respect to the AM, which becomes unacceptable for $k < 0.45$. Therefore, in order to ensure that both metrics lie below 1 dB, the deviation from a perfect 3 dB splitting ratio must be kept within ≈ 10 %. This coupling ratio tolerance is technologically feasible for commercially available PM 3 dB couplers. In fact, based on the specifications available for these components [49], even a change of up to 5 % from the optimal coupling condition is practically possible and would further improve the overall performance of the BFL. Also, we note that while k has no significant impact on the CT, it has a greater influence on the AM and the PP than θ. This is attributed to the different

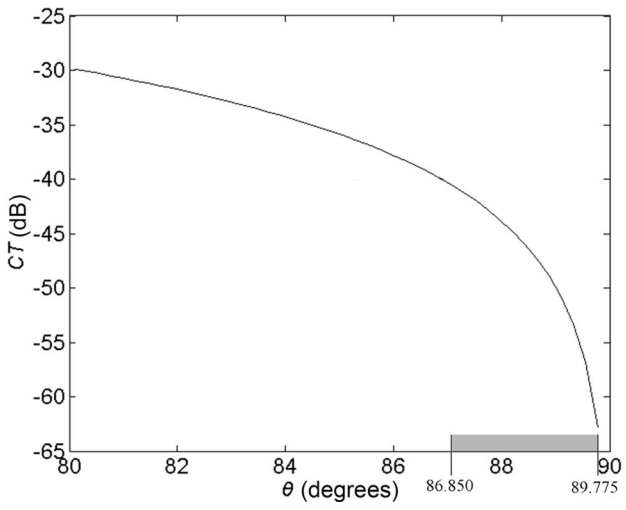

Fig. 7 Variation of crosstalk, *CT*, versus PC rotation angle, θ. The *gray zone* indicates the permissible range of values for this parameter

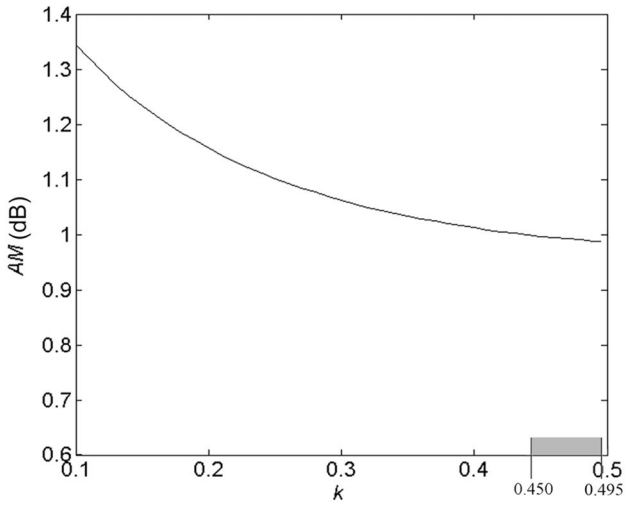

Fig. 8 Variation of amplitude modulation, AM, versus OC power splitting ratio, k. The *gray zone* indicates the permissible range of values for this parameter

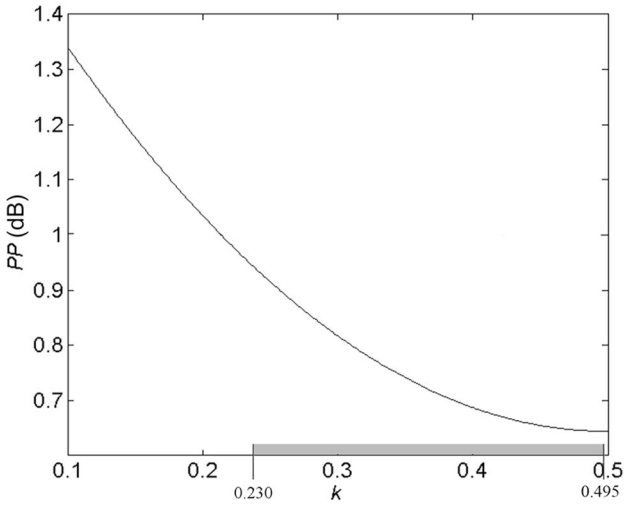

Fig. 9 Variation of power penalty, PP, versus OC power splitting ratio, k. The *gray zone* indicates the permissible range of values for this parameter

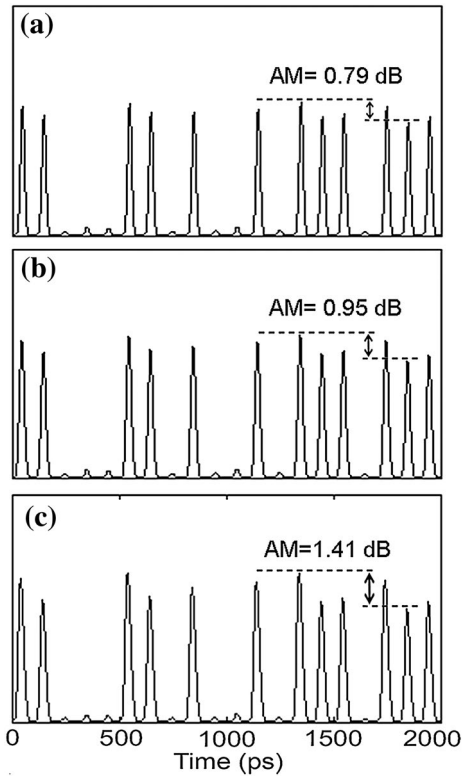

Fig. 10 Simulated temporal waveforms at BFL output for BFL critical performance parameters values assigned within, **a**, **b**, or outside, **c**, specified tolerance range. **a**, **b** refer to the best and worst-case scenarios, respectively

way these two parameters affect the BFL transfer function. Thus, θ affects the maximum peak, while k the maximum depth, of the transfer function. However, the influence of k is more intense than θ, because, according to (9), in the first case, the magnitude variation is parabolic-like, i.e., $4k^2 - 4k + 1$, while in the second case, it scales with the squared modulus of $\sin(\cdot)$. Consequently, the changes of θ within the range scanned in Fig. 7 affect negligibly the values of the transfer function, while those of k can cause a variation of up to 50 %. Since the data carrier is spectrally offset from the transmission peak [13, 14], the peak drop due to θ is a form of loss that does not impair the capability of suppressing the pattern effect. In contrast, what is important is to make the notch deep enough so that the red shifted SPM components of the amplified signal, which fall close to this notch, are sufficiently attenuated depending on the degree of their shift [15]. Meeting this requirement is decisively determined by k, so this parameter is more critical for the BFL performance tolerance compared to θ.

The outcome of the extensive analysis conducted above impacts the amplified data pulses as shown in Fig. 10. This figure depicts how the quality of these pulses, which belong to the same data frame as in Fig. 3, is affected when the BFL critical parameters lie (Fig. 10a, b), or not (Fig. 10c), within their specified tolerance range. We distinguish between the best (Fig. 10a) and worst (Fig. 10b) scenarios, which hold when the values assigned to these parameters coincide with their feasible upper and lower permissible limit, i.e., $(\Delta\tau, \theta, k) = (10.33\,\text{ps}, 89.775°, 0.475)$ and $(\Delta\tau, \theta, k) = (7.61\,\text{ps}, 86.85°, 0.45)$, respectively. In both cases, we verify that as long as the extracted operating conditions are satisfied, the AM stays below 1 dB, which is reflected on the maximum peak amplitude difference denoted by the vertical arrows. The same happens for the PP, which does not exceed 0.48 dB and in the most favorable situation is negligible. The CT is also less than 40 dB. These results are supported by a net gain of the BFL-SOA system [15] over 13 dB, which is adequate for direct signal amplification applications [15]. However, if the BFL is not designed according to the rules derived for its components, then the SOA pattern effect becomes harmful. In fact, all performance metrics become unacceptable, and intense peak amplitude fluctuations occur on the amplified pulses (Fig. 10c). This contrast between Fig. 10a–c shows the usefulness of the theoretical treatment in the effort to implement a BFL, which under real building circumstances manages to effectively reduce the SOA pattern effect.

6 Conclusion

In conclusion, we have presented a detailed study on the performance tolerance of a BFL employed to suppress the pattern effect in a SOA configured for direct signal amplification. A comprehensive model was used to describe the

BFL output in the general case that the settings of the BFL building components are not perfect. The model was validated by comparison to experimental data and was used to obtain simulation results to assess the impact of specified critical operating parameters on various performance metrics. It was shown that the performance of the conventional BFL is primarily affected by changes of $\Delta\tau$, then k, and finally, θ. In fact, variations of $\Delta\tau$ may be responsible for violating the defined criteria both for AM and PP, which also happens for k but to a comparatively lower extent. For θ, in contrast, only CT is significantly affected. Consequently, the degree of BFL performance tolerance is higher against fluctuations of θ, lower against deviations of k, and weaker against modifications of $\Delta\tau$. The BFL performance robustness against changes of these critical parameters can be enhanced if the BFL is constructed from special components, such as a programmable DGDL or PCF, a dynamically controlled PC, and a loop forming coupler fabricated with the least possible error from the absolutely even splitting ratio. This BFL construction is more cumbersome than the conventional one but technologically feasible. This fact combined with the attractive features of the BFL renders the latter a viable and efficient solution for combating the deleterious consequences of the SOA pattern effect with increased performance tolerance. Therefore, the BFL-based scheme can enhance the performance of SOAs in a variety of direct amplification applications, such as power boosting at the transmitter side [50, 51], in-line amplification along a fiber link [52, 53], and preamplification at the receiver end [54, 55].

Acknowledgments This work was supported in part by national research project Massive co-financed by the European Union (European Social Fund-ESF) and Greek national funds through the Operational Program Education and Lifelong Learning of the National Strategic Reference Framework (NSRF)-Research Funding Program: ARCHIMEDES III. Investing in knowledge society through the European Social Fund.

References

1. Y. Zhao, T.T. Song, Q. Wang, Instr. Sci. Technol. **40**(4), 239 (2012)
2. S. Ma, W. Li, H. Hu, N.K. Dutta, Opt. Commun. **285**(12), 2832 (2012)
3. M.P. Fok, W.W. Tang, C. Shu, Opt. Express **13**(12), 4752 (2005)
4. Y.W. Lee, J. Jung, B. Lee, IEEE Photon. Technol. Lett. **16**(1), 54 (2004)
5. G. Sun, Y. Zhou, Y. Hu, Y. Chung, Opt. Fiber Technol. **17**(1), 79 (2011)
6. C.W. Chow, C.S. Wong, H.K. Tsang, IEEE Photon. Technol. Lett. **17**(3), 693 (2005)
7. F. Wang, Y. Yu, X. Huang, X. Zhang, Opt. Commun. **282**(12), 2292 (2009)
8. B.E. Olsson, P. Ohlen, L. Rau, D.J. Blumenthal, IEEE Photon. Technol. Lett. **12**(7), 846 (2000)
9. C.W. Chow, H.K. Tsang, IEEE Photon. Technol. Lett. **17**(6), 1313 (2005)
10. B.E. Olsson, P.A. Andrekson, IEEE Photon. Technol. Lett. **9**(6), 764 (1997)
11. Q. Wang, H. Dong, G. Zhu, H. Sun, J. Jaques, A.B. Piccirilli, N. Dutta, Opt. Commun. **260**(1), 81 (2006)
12. O. Frazão, J.M. Baptista, J.L. Santos, Sensors **7**(11), 2970 (2007)
13. K.E. Zoiros, C. O'Riordan, M.J. Connelly, IEEE Photon. Technol. Lett. **22**(4), 221 (2010)
14. K.E. Zoiros, C. Riordan, M.J. Connelly, in *Conference on Networks and Optical Communications (NOC)*, p. 141 (2011)
15. Z.V. Rizou, K.E. Zoiros, A. Hatziefremidis, M.J. Connelly, J. Sel, Top. Quantum Electron. **19**(5), 1 (2013)
16. D.R. Zimmerman, L.H. Spiekman, J. Lightwave Technol. **22**(1), 63 (2004)
17. G.P. Agrawal, N.A. Olsson, IEEE J. Quantum Electron. **25**(11), 2297 (1989)
18. K. Inoue, Electron. Lett. **33**(10), 885 (1997)
19. T. Watanabe, H. Yasaka, N. Sakaida, M. Koga, IEEE Photon. Technol. Lett. **10**(10), 1422 (1998)
20. J. Yu, P. Jeppesen, J. Lightwave Technol. **19**(9), 1316 (2001)
21. C.S. Wong, H.K. Tsang, Opt. Commun. **232**(1–6), 245 (2004)
22. K.E. Zoiros, T. Siarkos, C.S. Koukourlis, Opt. Commun. **281**(14), 3648 (2008)
23. J. Dong, X. Zhang, F. Wang, W. Hong, D. Huang, Opt. Commun. **281**(22), 5618 (2008)
24. K. Hussain, R. Pradhan, P.K. Datta, Opt. Quantum Electron. **42**(1), 29 (2010)
25. E.A. Kuzin, H.C. Núñez, N. Korneev, Opt. Commun. **160**(1–3), 37 (1999)
26. P. Ma, N. Song, J. Jin, J. Song, X. Xu, Opt. Laser Technol. **44**(6), 1829 (2012)
27. C.S. Kim, Y.G. Han, R.M. Sova, U.C. Paek, Y. Chung, J.U. Kang, IEEE Photon. Technol. Lett. **15**(2), 269 (2003)
28. X. Ma, Z. Wu, G. Kai, Y. Liu, L. Liu, H. Zhang, S. Yuan, X. Dong, Opt. Fiber Technol. **12**(1), 1 (2006)
29. G. Qiao, Z. Cao, R. Wang, X. Ji, B. Gao, J. Peng, F. Xu, B. Yu, Opt. Commun. **285**(12), 2836 (2012)
30. R.M. Silva, A. Layeghi, M.I. Zibaii, H. Latifi, J.L. Santos, O. Frazão, J. Lightwave Technol. **30**(8), 1032 (2012)
31. G. Chen, J.U. Kang, J. Opt. A Pure Appl. Opt. **6**(4), 361 (2004)
32. C.S. Kim, B. Choi, J.S. Nelson, Q. Li, P.Z. Dashti, H.P. Lee, Opt. Lett. **30**(1), 20 (2005)
33. J. Bogdanski, J. Ahrens, M. Bourennane, Opt. Express **17**(6), 4485 (2009)
34. L. Xu, V. Baby, I. Glesk, P.R. Prucnal, Opt. Commun. **244**(1–6), 199 (2005)
35. R.C. Jones, J. Opt. Soc. Am. A. **31**(7), 488 (1941)
36. K. Morito, M. Ekawa, T. Watanabe, Y. Kotaki, J. Lightwave Technol. **21**(1), 176 (2003)
37. K.E. Zoiros, Z.V. Rizou, M.J. Connelly, Opt. Commun. **284**(14), 3539 (2011)
38. D.K. Mynbaev, L.L. Scheiner, *Fiber-Optic Communications Technology*, 1st edn. (Prentice-Hall, New Jersey, 2001), p. 189
39. G.P. Agrawal, *Fiber-Optic Communication Systems*, 3rd edn. (Wiley, New York, 2002)
40. R. Ramaswami, K.N. Sivarajan, *Optical Networks: A Practical Perspective*, 2nd edn. (Morgan Kaufmann Publishers, San Fransico, 2002)
41. G. Toptchiyski, S. Randel, K. Petermann, S. Diez, E. Hilliger, C. Schmidt, C. Schubert, R. Ludwig, H.G. Weber, J. Lightwave Technol. **18**(12), 2188 (2000)
42. J. Xu, X. Zhang, J. Mørk, IEEE J. Quantum Electron. **46**(1), 87 (2010)
43. F.J. MacWilliams, N.J.A. Sloane, Proc. IEEE **64**(12), 1715 (1976)

44. S. Singh, R.S. Kaler, Opt. Commun. **266**(1), 100 (2006)
45. J. Villatoro, V. Finazzi, V.P. Minkovich, V. Pruneri, G. Badenes, Appl. Phys. Lett. **91**(9), 091109/1 (2007)
46. M.A. Mirza, G. Stewart, in *Conference on Applied Sciences and Technology (IBCAST)*, p. 72 (2009)
47. See for instance the specifications for "Programmable Differential Group Delay Module". http://www.generalphotonics.com
48. See for instance the specifications for "Lightwave Polarization Controller". http://www.fiberpro.com
49. See for instance the specifications for "Polarization Maintaining Fused Coupler". http://www.jdsu.com
50. Y. Kim, H. Jang, Y. Kim, J. Lee, D. Jang, J. Jeong, J. Lightwave Technol. **21**(2), 476 (2003)
51. X. Wei, Y. Su, X. Liu, J. Leuthold, S. Chandrasekhar, IEEE Photon. Technol. Lett. **16**(6), 1582 (2004)
52. R. Gutiérrez-Castrejón, A. Filios, J. Lightwave Technol. **24**(12), 4912 (2006)
53. S. Boscolo, R. Bhamber, S.K. Turitsyn, V.K. Mezentsev, V.S. Grigoryan, Opt. Commun. **266**(2), 656 (2006)
54. P. Torres-Ferrera, R. Gutiérrez-Castrejón, Opt. Fiber Technol **20**(3), 177 (2014)
55. S. Singh, Opt. Commun. **284**(3), 828 (2011)